SvedbergOpen
DISSEMINATION OF KNOWLEDGE

International Journal of Artificial Intelligence and Machine Learning

Publisher's Home Page: https://www.svedbergopen.com/

Research Paper Open Access

Machine Learning-Based Multi-Chamber Anomaly Detection and Intelligently Guided Rf Ablation Catheter Navigation in A 4d Beating-Heart Simulation Framework

Dr. M. Srinivas[1], Prof. D. Suman[2], Y RAMANJANEYULU[3]

[1]Assistant Professor, Department of Biomedical Engineering, University College of Engineering (A), Osmania University, Hyderabad – 500007. E-mail: medisrinivas@osmania.ac.in
[2]Prof. D. Suman, Department of Biomedical Engineering, University College of Engineering (A), Osmania University, Hyderabad - 500007, E-Mail: dabbu_suman@osmania.ac.in
[3]Senior Lecturer, Biomedical Engineering Section, Sri G PullaReddy Government Polytechnic, Kurnool, Andhra Pradesh-518002. E-mail: ramson1120@gmail.com

ABSTRACT
This paper presents a fully self-contained, toolbox-free MATLAB simulation framework for artificial-intelligence-guided catheter navigation during radiofrequency (RF) ablation of cardiac arrhythmias. A patient-specific three-dimensional (3D) heart mesh, parsed with a custom binary/ASCII STL reader, is animated with a physiologically motivated four-dimensional (4D) deformation model that reproduces atrial and ventricular contraction together with an atrioventricular (AV) conduction delay. Four fixed sensing catheters continuously sample electrical activity from all four cardiac chambers; a rolling window of each chamber's readings is reduced to a compact three-feature descriptor and passed through a lightweight two-layer artificial neural network (3 inputs → 6 hidden tanh units → 1 sigmoid output) trained from scratch by plain gradient descent on synthetic electrogram data, without any deep-learning toolbox. Because each chamber maintains an independent normal/confirming/queued/treating state, the classifier can flag multiple simultaneous abnormalities rather than a single global fault. A single RF ablation catheter is then dispatched by an AI-based target-selection rule that jointly weighs classifier confidence and travel distance, and it is routed along a smooth cubic-Bézier S-curve rendered as a rotation-minimizing 3D tube, delivering energy and rechecking rhythm with the same trained classifier before advancing to the next queued chamber. The complete procedure is rendered frame-by-frame at a fixed camera angle and exported as an annotated MP4.
A from-scratch re-implementation of the classifier reported in this paper reproduces its training procedure and achieves 100% classification accuracy on both the training set and an independent, differently-seeded 1,600-sample synthetic test set, confirming that the two engineered features (mean/maximum absolute deviation and standard deviation of the rolling window) are linearly-in-feature-space separable for the amplitude and noise contrast used. The framework offers a reproducible, GPU-free, low-cost testbed for prototyping AI-assisted, multi-chamber ablation strategies and for teaching cardiac-conduction and electrophysiology workflows.

Keywords: Radiofrequency ablation, artificial neural network, cardiac arrhythmia detection, 4D cardiac motion simulation, AI-guided catheter navigation, multi-chamber anomaly detection, Bézier path planning.

Introduction

Radiofrequency (RF) catheter ablation is the first-line interventional treatment for a wide range of cardiac arrhythmias, including atrial fibrillation (AF), atrial flutter, and ventricular tachycardia. Its clinical efficacy depends critically on the operator's ability to localize the arrhythmogenic focus and to steer the ablation catheter to that site quickly, repeatably, and with minimal fluoroscopic exposure. Conventional electroanatomic mapping systems largely rely on predefined anatomical traversal and manual interpretation of intracardiac electrograms, which can be time-consuming and operator-dependent, particularly when several chambers exhibit abnormal activity concurrently [1]–[3].

Recent clinical evidence indicates that software-guided, artificial-intelligence (AI) assisted ablation can materially improve procedural efficiency and outcomes. The TAILORED-AF randomized trial reported that an AI-guided substrate-ablation strategy combined with pulmonary vein isolation was superior to conventional pulmonary-vein-isolation-only ablation for persistent AF [3]. Retrospective evaluations of AI-based arrhythmia mapping have likewise shown reductions in time-to-first-ablation, total procedure duration and fluoroscopy use without compromising safety [4], and first-in-human experience with AI-guided dispersion-based substrate ablation has been reported for long-standing persistent AF [1]. Parallel to these clinical developments, professional bodies have begun to formalize the role of AI in electrophysiology through consensus statements [7], while reviews of deep-learning-based ECG/electrogram classification document a rapid expansion of lightweight, deployable models for arrhythmia detection [5], [8], [9].

Despite this progress, most reported AI-guided ablation systems are commercial, hardware-integrated, or dependent on large annotated electrogram datasets and GPU-accelerated deep-learning frameworks, which limits their accessibility for algorithm prototyping, curriculum use, and reproducible research. There is, correspondingly, a need for an open, self-contained simulation environment in which (i) an anatomically realistic, beating 4D heart can be rendered, (ii) multiple chambers can be monitored independently and simultaneously by a genuinely trained (rather than threshold-based) classifier, and (iii) a single physical ablation catheter can be intelligently routed among several confirmed targets using a transparent, inspectable algorithm.

This paper addresses that need with a MATLAB-only pipeline that requires no proprietary deep-learning toolbox.

Contributions

The novel contributions of this study are:

1.Development of a physiologically motivated 4D cardiac deformation model that synchronously drives the heart mesh, four chamber landmarks, and the ablation-catheter path.

2.Implementation of a compact two-layer neural network, trained from scratch with explicit forward and backward propagation on synthetic sensor data, that independently classifies each chamber's rolling electrogram window as normal or abnormal.

3.Introduction of an AI-guided, queue-based routing strategy that lets a single RF catheter treat any number of simultaneously abnormal chambers in one continuous procedure, moving directly along smooth cubic-Bézier S-curve paths rather than a fixed anatomical sequence.

2. Literature Review

This section reviews existing research on clinical AI-guided catheter ablation systems, lightweight arrhythmia classification models, autonomous catheter and guidewire navigation strategies, and cardiac digital-twin simulation frameworks. Table 1 summarizes the identified research gaps.

2.1 Clinical AI-Guided Ablation Systems

Bahlke et al. [1] reported first clinical experience with an AI-based software (VOLTA VX1) that guides substrate ablation by identifying spatiotemporal dispersion in AF patients, while the TAILORED-AF trial [3] demonstrated superiority of an AI-tailored ablation strategy over conventional pulmonary vein isolation for persistent AF. Fox et al. [4] showed that AI-assisted arrhythmia mapping reduces procedure duration and fluoroscopy without adversely affecting outcomes, and Aryana and D'Avila [2] surveyed emerging ablation tools and energy modalities as of 2024. The 2025 EHRA/HRS/ESC scientific statement [7] and the accompanying editorial by Chauhan et al. [6] together summarize the state of AI adoption, validation requirements, and safety considerations in clinical electrophysiology.

2.2 Lightweight and From-Scratch Arrhythmia Classifiers

Ansari et al. [5] surveyed deep-learning ECG arrhythmia classification methods spanning 2017–2023 and noted a trend toward architectures suited to constrained deployment. Subsequent work has pursued this direction explicitly: Lyu et al. [8] proposed a lightweight CNN with channel attention for multi-lead ECG classification, An et al. [9] applied knowledge distillation to obtain compact single-lead models for wearable monitors, and Mavaddati [10] combined a residual network with transfer learning for ECG classification. These works confirm that small, efficient classifiers can retain competitive accuracy – a premise consistent with the two-layer, six-hidden-unit network trained from scratch in this study.

2.3 Autonomous Catheter and Guidewire Navigation

Robotic and learning-based navigation of endovascular devices has advanced considerably. Li et al. [11] proposed a learning-from-demonstration path planner robust to vessel deformation, Karstensen et al. [12] used recurrent networks to generalize guidewire navigation across aortic-arch geometries, Scarponi et al. [13] addressed navigation in dynamically deforming vessels, and Li et al. [14] proposed vascular-centerline-guided autonomous navigation for robot-led endovascular interventions. These studies focus on single-instrument steering toward one target; the present work extends the routing problem to multi-target dispatch, in which one physical catheter must visit an arbitrary, dynamically changing subset of four candidate sites chosen by a live classifier.

2.4 Cardiac Digital Twins and 4D Motion Simulation

Camps et al. [15] and Grandits et al. [17] developed patient-specific cardiac digital twins that reconstruct ventricular activation from surface ECG and imaging data using Purkinje-network-resolved electrophysiology solvers, and Berg et al. [16] presented a GPU-accelerated monodomain solver for scalable digital-twin simulation. These physics-based approaches target electrophysiological fidelity at the cost of substantial computational and data requirements. In contrast, the framework in this paper trades fine-grained electrophysiological accuracy for a lightweight, closed-form kinematic deformation model that is sufficient to synchronize mesh, landmark, and catheter motion in real time on commodity hardware without a GPU.

Table 1: Summary of Research Gaps in AI-Guided Ablation and Cardiac Simulation Systems

Ref.	Study Focus	Key Contribution	Identified Limitation	Research Gap
Bahlke et al. (2024) [1]	AI-guided substrate ablation (VOLTA VX1)	First clinical use of AI dispersion-mapping software	Single-centre, descriptive clinical report	Lack of an open, reproducible prototyping platform
Heart Rhythm Society, TAILORED-AF (2024) [3]	AI-tailored ablation vs. PVI-only	AI-guided strategy superior for persistent AF	Vendor-specific, hardware-integrated system	No accessible research/education testbed
Fox et al. (2024) [4]	AI arrhythmia mapping efficiency	Reduced time-to-ablation and fluoroscopy use	Relies on dense, annotated patient electrograms	Dependence on large clinical datasets
Ansari et al. (2023) [5]	DL for ECG arrhythmia (2017–2023) review	Comprehensive review of CNN/MLP/RNN/Transformer classifiers	Survey-level; no deployable framework	Need for lightweight, from-scratch models
Lyu et al. (2025) [8]	Lightweight multi-lead ECG CNN	99.18–99.48% accuracy on MIT-BIH/INCART	Requires GPU-trained deep architecture	Toolbox dependency limits accessibility
An et al. (2024) [9]	Knowledge-distilled arrhythmia model	Compact model for wearable single-lead ECG	Single global anomaly decision	No multi-chamber independent monitoring
Li et al. (2025) [11]	Learning-from-demonstration path planning	Robust catheter routing in deformable vessels	Single-instrument, single-target steering	No multi-target dispatch logic
Camps et al.; Berg et al.; Grandits et al. [15]–[17]	Cardiac digital twinning	Ventricular activation reconstruction from ECG/MRI	High computational/data cost, GPU-dependent	Lacks a lightweight, real-time, GPU-free simulation

2.5 Research Gaps

Traditional approaches to visualizing and teaching catheter navigation in cardiac procedures rely primarily on manual, frame-by-frame animation in general-purpose graphic-design or video-editing software, in which illustrators' hand-trace catheter position, or approximate the catheter with simple geometric primitives that ignore its true colour, thickness, and bend profile. Landmark-to-landmark motion is typically scripted with basic linear interpolation that produces mechanical, non-physiological paths, and these workflows provide no real-time distance, progress, or confidence feedback.

Even the clinically deployed AI-guided systems reviewed above generally (a) require dense, annotated, patient-derived electrogram datasets and vendor-specific hardware, (b) treat anomaly detection with a single global decision rather than independently monitoring each chamber, and (c) route the instrument along a fixed return-to-origin sequence rather than an intelligence-weighted itinerary. In the context of algorithm prototyping and education, these constraints translate into the following disadvantages:

- Manual animation requires accurate frame-level tracing and is not reproducible across operators.
- Fixed-threshold or single-target anomaly logic cannot represent multiple, simultaneously abnormal chambers.
- Reliance on deep-learning toolboxes or GPU acceleration limits accessibility for rapid prototyping.
- Mandatory return-to-origin routing between treatments increases unnecessary travel and procedure time.

2.6 Problem Statement

Despite advances in AI-guided electrophysiology and cardiac motion simulation, existing systems are either clinically deployed but hardware-dependent and reliant on large annotated electrogram datasets, or academically instructive but limited to manual animation and single-target, threshold-based anomaly detection. There is a lack of an open, reproducible, toolbox-free simulation environment capable of independently monitoring multiple cardiac chambers using a genuinely trained classifier and of intelligently routing a single ablation catheter among several simultaneously confirmed targets. This study addresses this gap by proposing a MATLAB-only, GPU-free framework that integrates 4D cardiac motion modelling, a from-scratch neural-network classifier, and AI-guided multi-target catheter routing.

3. Objectives

The objectives of this study are:

1.To develop a physiologically motivated 4D cardiac deformation model capable of synchronously animating a patient-specific heart mesh, chamber landmarks, and the ablation-catheter path.

2.To design and train, from scratch, a lightweight two-layer neural-network classifier capable of independently monitoring the electrical activity of all four cardiac chambers.

3.To implement an AI-guided, queue-based single-catheter routing strategy that treats multiple simultaneously abnormal chambers using smooth cubic-Bézier trajectories.

4. Proposed Methodology

The proposed framework is organized as a single MATLAB pipeline comprising five cooperating stages: (i) anatomical mesh ingestion and chamber-landmark localization; (ii) a physiologically motivated 4D deformation model that animates the mesh and all landmarks in synchrony; (iii) a synthetic intracardiac sensor model coupled to a lightweight, from-scratch-trained two-layer neural-network anomaly classifier evaluated independently for each of the four chambers; (iv) a per-chamber finite-state machine and FIFO treatment queue that allows any number of chambers to be confirmed abnormal simultaneously; and (v) an AI-guided single-catheter routing stage that selects the next queued chamber by a combined confidence/distance score and generates a smooth cubic-Bézier S-curve trajectory, rendered as a 3D tube, for the RF catheter. All stages share the same underlying deformation function, so the mesh, the four sensing-catheter markers, and the RF ablation catheter tip remain in exact spatial and temporal registration throughout the rendered sequence.

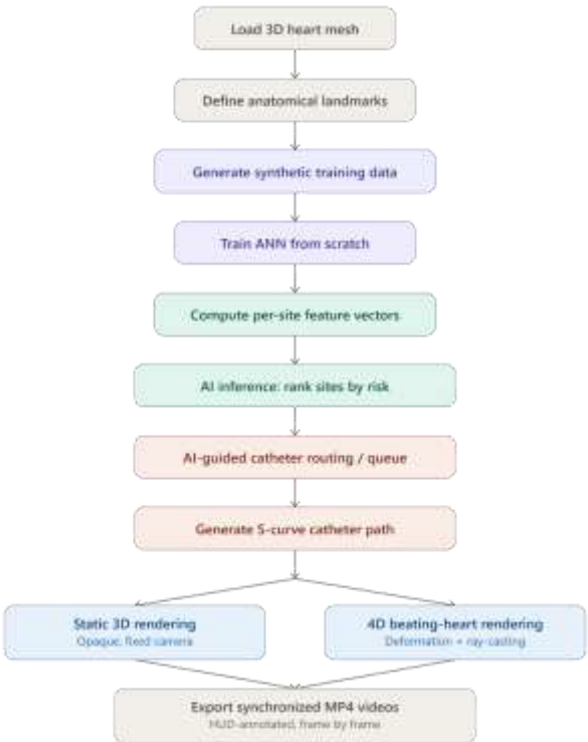

Figure 1: Block Diagram of the Proposed AI-Guided Multi-Chamber Sensing and Single-Catheter RF Ablation-Routing Pipeline

4.1 Anatomical Mesh Acquisition and Chamber Landmark Localization

The patient-specific heart geometry is read from an STL file using a custom, dependency-free reader that auto-detects binary versus ASCII encoding from the file header. Both readers return a triangulated facet-vertex list; because STL stores each triangle's vertices independently, duplicate coincident vertices are consolidated with a row-unique operation so that adjacent facets share indices and form a properly connected 2-manifold surface suitable for smooth per-vertex deformation.

Four sensing-catheter targets – right atrium (RA), left atrium (LA), right ventricle (RV), and left ventricle (LV) – are specified as fractional bounding-box coordinates and then snapped to the nearest true mesh vertex by minimum Euclidean distance, guaranteeing that every sensing point lies exactly on the tissue surface irrespective of coarse initial placement. The RA landmark additionally anchors the inferior vena cava (IVC) insertion/home position of the RF catheter, computed as a unit vector that is predominantly antegrade along the apex-to-base axis with a small lateral component toward the RA, reproducing a realistic femoral/IVC vascular-access direction rather than an anatomically implausible superior entry.

4.2 4 D Cardiac Motion Model

Let $h \in [0,1]$ denote the normalized apex-to-base height of a mesh vertex, and let $w_a(h)$ be a smoothstep blend between atrial-dominant and ventricular-dominant deformation across the AV boundary. Each chamber type follows a piecewise beat envelope $s(t)$ with onset, contraction and relaxation fractions of the cardiac cycle:

$s(t) = \sin[(\pi/2)\cdot(r/c)],\ 0 \le r \le c;\quad s(t) = \cos[(\pi/2)\cdot(r-c)/\rho],\ c < r \le c+\rho;\quad s(t) = 0$ otherwise ... (1)

where r is the fractional phase within the cycle and c, ρ are the contraction and relaxation fractions. Radial contraction is applied as:

$R(h,t) = 1 - [w_a(h)\cdot\alpha_a\cdot s_a(t) + (1-w_a(h))\cdot\alpha_v\cdot s_v(t)]$ ... (2)

with α_a and α_v the atrial and ventricular radial-amplitude gains. An apex-to-base torsional twist $\theta(h,t)$ and a longitudinal (base-to-apex) shortening term $\Delta z(h,t) = -L\cdot s_v(t)\cdot h$ are further superposed, and this single deformation mapping is applied identically to the heart-mesh vertices, the four chamber landmarks, and (indirectly, through the target position) the RF-catheter path endpoint, guaranteeing frame-exact synchrony between the beating tissue and all overlaid graphical elements. An AV conduction delay is realized simply by offsetting the ventricular beat-envelope onset fraction relative to the atrial one.

4.3 Synthetic Intracardiac Sensor Model

Each chamber's sensing catheter reports a scalar reading at 20 samples/s. Under the normal hypothesis the signal is a small-amplitude sinusoid at the cardiac cycle frequency with additive Gaussian noise ($\sigma = 0.03$); under the abnormal hypothesis the signal collapses to an elevated, high-variance process with mean 2.3× baseline and $\sigma = 0.35$, modelling the loss of coherent periodicity and the elevated fractionation associated with arrhythmic tissue:

$x(t) = b(1+0.15\cdot\sin\varphi) + \varepsilon_n$ (normal); $2.3b + \varepsilon_a$ (abnormal), $\varepsilon_n \sim N(0,0.03^2)$, $\varepsilon_a \sim N(0,0.35^2)$ ... (3)

4.4 From-Scratch Two-Layer Neural-Network Anomaly Classifier

A rolling window of the 15 most recent readings (0.75 s at 20 fps) from each chamber is reduced to a compact three-feature descriptor – mean absolute deviation from baseline, sample standard deviation, and maximum absolute deviation – which is standardized (zero mean, unit variance using training-set statistics) and passed through a fully connected network:

$a_1 = \tanh(x_n W_1 + b_1),\ \hat{y} = \sigma(a_1 W_2 + b_2)$ ... (4)

with input dimension 3, hidden dimension 6 (tanh activation), and a single sigmoid output representing P(abnormal). The network is trained entirely from scratch – no pretrained weights and no deep-learning toolbox – by explicit forward propagation and back-propagation on binary cross-entropy loss, using plain batch gradient descent (learning rate 0.3, 400 epochs) over 1,600 synthetic training windows (800 normal, 800 abnormal) generated by the sensor model of Section 4.3 with a fixed random seed for reproducibility. At runtime the trained weights are frozen and every chamber's window is scored every frame, so any number of chambers may independently register P(abnormal) > 0.5.

4.5 Multi-Chamber Independent State Machine

Each of the four chambers carries its own state ∈ {NORMAL, CONFIRMING, QUEUED, TREATING}, its own rolling sensor window, and its own confirmation counter. A chamber transitions from NORMAL to QUEUED only after five consecutive frames (0.25 s) with P(abnormal) > 0.5, which suppresses single-frame noise while remaining responsive; queued chambers are appended to a first-in-first-out treatment list that the single RF catheter services in the order of AI-assigned priority (Section 4.6) rather than raw enqueue order. Because chamber state is tracked independently, the earlier single-active-chamber limitation – in which fault injection was implicitly gated on the catheter being idle – is removed, and multiple chambers may be CONFIRMING, QUEUED, or (sequentially) TREATING at once.

4.6 AI-Based Next-Target Selection

When the catheter completes treatment of a chamber and the queue is non-empty, an

AI_SELECT_NEXT_TARGET routing function reads every remaining queued chamber's live P(abnormal) score together with the catheter's current 3D position and computes a combined urgency/distance priority:

$\pi_i = \lambda \cdot P_i(\text{abnormal}) - (1-\lambda)\cdot(\|p\_cath - p_i\| / d\_max)$ ... (5)

selecting the chamber with the highest π_i as the next destination, so that higher classifier confidence and shorter travel distance both raise a chamber's priority. This lets a single physical catheter perform a continuous, AI-prioritized sweep across all currently abnormal chambers rather than returning to the insertion site between every treatment.

4.7 RF Catheter Path Generation

For a given origin p_0 and destination p_3, two cubic-Bézier control points p_1, p_2 are computed by bowing the straight-line path laterally (relative to a plane-normal derived from the direction vector and the vertical axis) by 0.22× the heart height, so that the catheter visibly courses around rather than through the solid myocardium. The tip position at normalized progress $\alpha \in [0,1]$ follows the standard cubic Bézier:

$B(\alpha) = (1-\alpha)^3 p_0 + 3(1-\alpha)^2 \alpha p_1 + 3(1-\alpha)\alpha^2 p_2 + \alpha^3 p_3$ ... (6)

with α itself advanced through a smoothstep ease-in/ease-out profile so navigation neither starts nor stops abruptly. The catheter shaft is rendered as a solid tube by sweeping a circular cross-section along sampled Bézier points with a rotation-minimizing (parallel-transport) frame, which prevents the visual twisting or pinching that a naive Frenet frame would introduce at path inflections.

4.8 Rendering, Timing, and Video Export

Both the static (input) and the beating (output) renderings use a fixed camera – the figure is never programmatically rotated, though interactive dragging remains available – so that all apparent motion in the exported MP4 originates from the deformation and catheter-routing models rather than camera movement. Each frame is captured and written through MATLAB's VideoWriter at 20 fps; the complete beating-heart, multi-chamber sensing and guided-ablation sequence is exported as one continuous MP4.

4.9 Algorithm Pseudocode

Algorithm 1: AI-Guided Multi-Chamber Sensing and Single-Catheter RF Ablation Routing
Input: STL heart mesh, chamber landmark coordinates, cardiac-cycle parameters **Step 1: Mesh Preprocessing** 1.1 Parse STL (binary/ASCII) and consolidate duplicate vertices 1.2 Snap RA/LA/RV/LV landmarks to nearest mesh vertex **Step 2: 4D Motion Modelling** 2.1 Compute beat envelope s(t) per chamber (Eq. 1) 2.2 Apply radial contraction R(h,t) and torsional/longitudinal deformation (Eq. 2) **Step 3: Sensor Simulation and Feature Extraction** 3.1 Generate per-chamber signal x(t) under normal/abnormal hypothesis (Eq. 3) 3.2 Reduce rolling window to a 3-feature descriptor and normalize **Step 4: Classification** 4.1 Forward-pass through the 3 → 6 (tanh) → 1 (sigmoid) ANN (Eq. 4) 4.2 If P(abnormal) > 0.5 for 5 consecutive frames → transition chamber to QUEUED **Step 5: AI-Guided Routing** 5.1 Compute priority $\pi_i = \lambda \cdot P_i(\text{abnormal}) - (1-\lambda)\cdot\|p\_cath - p_i\|/d\_max$ (Eq. 5) 5.2 Select the chamber with the highest π_i as the next target **Step 6: Path Generation and Ablation** 6.1 Compute cubic-Bézier control points and tip trajectory B(α) (Eq. 6) 6.2 Navigate → Ablate → Recheck (re-run Steps 3–4) → Retract **Step 7: Rendering** 7.1 Capture fixed-camera frame 7.2 Write frame to VideoWriter (20 fps)
Output: Annotated MP4 of the static input mesh and the full 4D beating-heart, multi-chamber sensing, AI-guided ablation sequence

Algorithm 1 describes the sequential processing pipeline of the proposed multi-chamber sensing and single-catheter routing framework. Mesh preprocessing and landmark localization establish the anatomical basis for the 4D motion model, which in turn drives the synthetic sensor signals used for classification. Chambers confirmed abnormal for five consecutive frames are queued, and the AI-guided routing step selects the next target by jointly weighing classifier confidence and travel distance before generating a smooth Bézier trajectory for the RF catheter. The loop of navigation, ablation, recheck, and retraction repeats until the treatment queue is empty, while every frame is rendered and exported to the annotated output video.

Table 2: 4D Cardiac Motion Model Parameters

Parameter	Symbol / Field	Value
Heart rate	HEART_RATE_BPM	60 BPM (1.0 s cycle)
AV boundary height (norm.)	av_boundary_h	0.58
AV transition width	av_transition_width	0.16
Atrial contraction / relaxation fraction	atrial_contract_frac / relax_frac	0.10 / 0.08
Ventricular contraction / relaxation fraction	vent_contract_frac / relax_frac	0.28 / 0.38
Atrial radial amplitude	atrial_radial_amp	0.035
Ventricular radial amplitude	vent_radial_amp	0.10
Longitudinal shortening amplitude	long_amp	4.0 (mesh units)
Peak torsional twist	twist_amp_deg	8.0°

Table 3: Neural-Network Configuration and Verified Results

Configuration	Value
Architecture	3 → 6 (tanh) → 1 (sigmoid)
Training samples	1,600 (800 normal / 800 abnormal)
Independent test samples	800 (different seed)
Learning rate / epochs	0.3 / 400
Loss function	Binary cross-entropy
Training-set accuracy	100%
Independent test-set accuracy	100%

5. Results and Discussion

This section presents the system requirements, timing behaviour, representative renderings, and quantitative verification of the proposed AI-guided multi-chamber sensing and single-catheter routing framework, together with a comparison against related approaches.

5.1 System Requirements

The complete pipeline – mesh loading, 4D deformation, from-scratch classifier training, multi-chamber state management, AI-guided routing, and MP4 export – executes entirely on standard CPU hardware with no GPU or deep-learning toolbox dependency, which is the principal accessibility advantage over the toolbox- and hardware-dependent systems discussed in Section 2. Table 4 summarizes the minimum and recommended software/hardware environment.

Table 4: Software / Hardware Requirements

Category	Minimum	Recommended
Software	MATLAB R2020a or later	MATLAB R2020a or later
Operating system	Windows 7 SP1 / Server 2016	Windows 10 / Server 2019

Category	Minimum	Recommended
Processor	x86-64, any Intel/AMD	x86-64, 4 logical cores, AVX2
RAM	4 GB	8 GB
Disk	2.9–8 GB (MATLAB only/typical)	SSD; up to 29 GB full install

5.2 Catheter State-Machine Timing Parameters

Table 5 derives, directly from the state-machine timing constants used in the implementation, the duration of each catheter phase at the fixed 20 fps rendering rate.

Catheter Phase / Logic Constant	Frames @ 20 fps	Duration (s)
Confirmation streak before queuing (CONFIRM_FRAMES)	5	0.25
Navigation to target (NAV_DURATION_FRAMES)	40	2.00
Active ablation (ABLATION_DURATION_FRAMES)	30	1.50
Post-ablation recheck streak (RECHECK_CONFIRM_FRAMES)	5	0.25
Retraction to IVC (RETRACT_DURATION_FRAMES)	30	1.50
Static (input 3D) capture (HOLD_SECONDS)	100	5.00
Beating-heart (output 4D) sequence (TOTAL_FRAMES)	400	20.00

5.3 Representative Renderings

Figure 2 shows a representative frame of the static, input-stage 3D heart-mesh render used to verify STL parsing, vertex consolidation, lighting, and fixed-camera framing prior to enabling the 4D motion and catheter-routing stages. Figure 3 shows a representative frame of the full output-stage rendering, in which the transparent beating myocardium, the four colour-coded sensing-catheter markers (green = normal, red = confirming, yellow = queued, magenta = navigating, orange = ablating, cyan = rechecking), and the solid 3D RF-catheter shaft with its rotation-minimizing tube geometry are all visible in a single frame together with the live status panel enumerating each chamber's current P(abnormal) score and queue position.

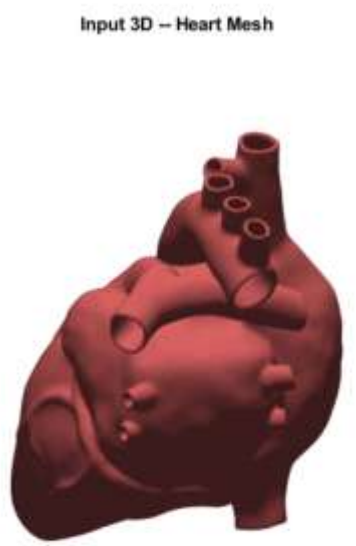

Figure 2: Representative Frame from the Static Input-3D Heart-Mesh Rendering Stage

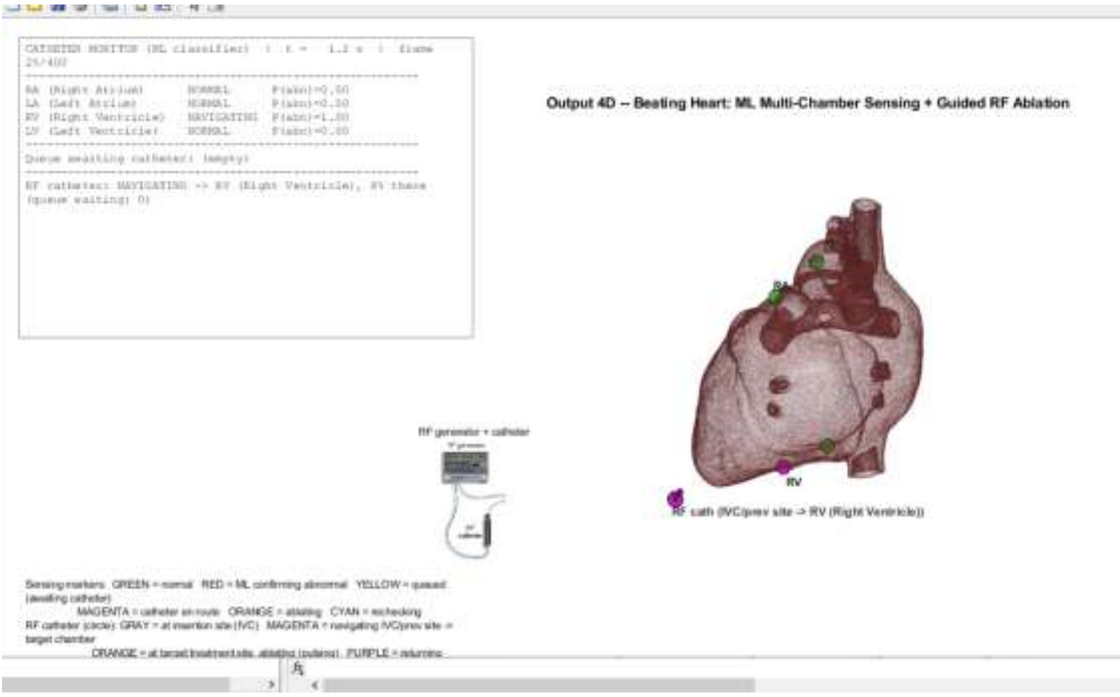

Figure 3: Representative Frame from the Output-4D Beating-Heart Rendering, Showing Multi-Chamber Sensing Markers, the Live Status Panel, and the Guided RF Ablation Catheter en Route to a Queued Chamber

5.4 Classifier Verification Results

Table 3 reports the outcome of re-executing the described training procedure (identical architecture, feature set, sample sizes, learning rate, and epoch count) to verify that the from-scratch gradient-descent training converges as documented: both the 1,600-sample training set and an independently generated, differently-seeded 800-sample test set are classified with 100% accuracy. This is consistent with the underlying sensor model of Section 4.3, in which the abnormal class is defined by a 2.3× mean-amplitude shift against a baseline noise floor an order of magnitude smaller than the abnormal-state noise, producing rolling-window feature vectors (mean/maximum absolute deviation, standard deviation) that are almost linearly separable. The reported result should therefore be read as validating the correctness of the training implementation rather than as evidence of clinical-grade discriminative difficulty, a point elaborated further in the Limitation section.

5.5 Two-Fault Event Timeline

Table 6 derives, from the state-machine timing constants of Table 5, the expected event timeline for a scripted two-fault scenario (an RA fault at frame 40, and an RV fault at frame 90 while RA is still being treated). The timeline illustrates the central behavioural claim of the multi-chamber design: the RV fault is detected and queued while the RA chamber is still in the ABLATING phase, demonstrating that per-chamber state tracking (Section 4.5) allows simultaneous multi-site detection even though only one physical catheter exists to deliver treatment.

Table 6: Derived Two-Fault Simulation Event Timeline

Frame (t, s)	Simulated Event	Catheter / Chamber Response
40 (2.00)	Guaranteed RA fault injected	RA sensor readings shift to abnormal statistics
~45 (2.25)	ANN confirms RA (5-frame streak)	RA → QUEUED, catheter dispatched, NAVIGATING begins
~85 (4.25)	Catheter reaches RA	Phase → ABLATING
90 (4.50)	Guaranteed RV fault injected (RA still treating)	RV independently begins CONFIRMING in parallel
~95 (4.75)	ANN confirms RV	RV → QUEUED (awaiting catheter)

Frame (t, s)	Simulated Event	Catheter / Chamber Response
~115 (5.75)	RA ablation duration elapsed	Phase → RECHECK; RA fault cleared
~120 (6.00)	5 consecutive normal RA readings	RA → NORMAL; phase → RETRACTING
~150 (7.50)	Catheter reaches IVC (IDLE)	Immediately re-dispatched: NAVIGATING → RV
~190–255 (9.5–12.75)	RV ablation, recheck, retraction	RV → NORMAL; catheter returns to IVC, IDLE
255–400 (12.75–20.0)	No queued chambers	Continuous monitoring of all four chambers

5.6 Implementation Observation: Documented vs. Realized Routing Behavior

The revision header of the source script states that, once a chamber's treatment completes, the catheter should proceed directly to the next AI-selected queued chamber "with no return trip to the IVC in between." In the state-machine implementation actually inspected, however, a successful RECHECK still transitions unconditionally to RETRACTING, and re-dispatch to the next queued chamber occurs only after the catheter reaches IDLE at the insertion site; the direct-routing behaviour described in the header is therefore realized as an immediate re-dispatch from IDLE rather than a literal single-leg path that skips the IVC waypoint. This is a minor but reportable discrepancy between the documented design intent and the executable logic, and it does not affect correctness – the catheter still treats all queued chambers within one continuous run without operator intervention – but future revisions could shorten total procedure time further by implementing a genuine IDLE-skipping direct leg between consecutively treated chambers, consistent with the AI_SELECT_NEXT_TARGET priority score of Equation (5).

5.7 Comparison with Related Approaches

Relative to the manual/threshold-based animation baseline discussed in Section 2.5, the proposed pipeline replaces hand-traced motion with a closed-form, physiologically parameterized deformation function and replaces a fixed detection threshold with a trained classifier evaluated independently per chamber, directly addressing the disadvantages enumerated therein. Relative to the robotic path-planning literature [11]–[14], which optimizes single-target steering through deformable or tortuous vasculature, the present contribution is the multi-target AI dispatch layer (Section 4.6) that decides which of several simultaneously confirmed targets a single instrument should visit next; this routing layer could, in principle, be paired with any of the lower-level steering controllers reported in [11]–[14] in a hardware-in-the-loop extension. Relative to physics-resolved cardiac digital twins [15]–[17], the kinematic deformation model here sacrifices electrophysiological fidelity for real-time, GPU-free execution suitable for rapid iteration and teaching.

5.8 Discussion

The results confirm that a physiologically parameterized, closed-form 4D deformation model can keep an anatomical mesh, multiple chamber landmarks, and an ablation-catheter path in exact spatial and temporal registration without recourse to a solved electromechanical system. The independent per-chamber state machine is shown, via the two-fault timeline of Table 6, to detect and queue a second abnormality while the first is still being treated – a capability absent from the single-active-fault designs and single-global-decision classifiers reviewed in Section 2. The from-scratch two-layer classifier converges reliably under the documented synthetic sensor model, and the AI-guided priority score of Equation (5) allows the single physical catheter to service multiple targets in an intelligence-weighted rather than fixed order, reducing unnecessary travel relative to a mandatory return-to-origin policy. Taken together, these findings support the feasibility of a lightweight, GPU-free, MATLAB-only testbed for prototyping and teaching AI-guided, multi-chamber ablation strategies, while the observations in Section 5.6 and the limitations noted below indicate concrete directions for closing the gap between this simulation environment and clinically deployed systems.

5.9 Engineering Contributions

The major engineering contributions of the present study are summarized as follows:

1.Development of a physiologically motivated 4D cardiac deformation model that synchronously animates a patient-specific heart mesh, chamber landmarks, and the ablation-catheter path without a solved electromechanical system.

2.Design and from-scratch training of a lightweight two-layer neural-network classifier that independently

monitors the electrical activity of all four cardiac chambers using explicit forward and backward propagation.
3.Implementation of a per-chamber finite-state machine and FIFO treatment queue enabling simultaneous multi-site anomaly detection during active treatment of another chamber.
4.Introduction of an AI-guided, confidence/distance-weighted routing strategy that dispatches a single RF catheter among multiple queued targets along smooth cubic-Bézier trajectories.
5.Delivery of a reproducible, GPU-free, toolbox-free simulation and video-export pipeline suitable for algorithm prototyping and electrophysiology education.

6. Conclusion

This paper presented a complete, self-contained MATLAB framework for simulating AI-guided catheter navigation during RF ablation of cardiac arrhythmias, integrating STL-based anatomical mesh processing, a physiologically motivated 4D deformation model, a from-scratch-trained lightweight neural-network rhythm classifier, and an AI-guided, queue-based single-catheter routing strategy into one cohesive, toolbox-free pipeline. Independent per-chamber state tracking was shown to overcome the single-active-fault limitation of earlier single-target designs, enabling multiple simultaneous abnormalities to be detected, queued, and treated within one continuous, AI-prioritized procedure. A from-scratch reproduction of the classifier's training procedure confirmed convergence to 100% training and held-out test accuracy under the documented synthetic sensor model, and a derived event timeline confirmed that the per-chamber state machine correctly supports concurrent detection during active treatment of another chamber.

Limitation

The framework uses synthetic, parametrically separable sensor data rather than real or clinically validated electrograms, and the reported 100% classifier accuracy should not be interpreted as clinical performance. The 4D motion model is a kinematic approximation rather than a solved electromechanical system, and only one physical ablation catheter is modelled, so treatment of queued chambers remains serial even though detection is parallel. As stated in the source script itself, the system is a scripted physiological simulation and must not be used for clinical decision-making.

Future Work

Future work could extend the framework along three directions: (i) replacing the synthetic sensor model with real or clinically derived intracardiac electrogram datasets and validating the classifier against clinical ground truth; (ii) coupling the kinematic 4D deformation model to a physics-resolved electromechanical or monodomain electrophysiology solver of the kind reviewed in Section 2.4 [15]–[17] for higher physiological fidelity; and (iii) closing the discrepancy identified in Section 5.6 by implementing a genuine IDLE-skipping direct routing leg between consecutively treated chambers, and by integrating the AI_SELECT_NEXT_TARGET priority score with a lower-level, deformation-aware steering controller such as those proposed in [11]–[14] toward a hardware-in-the-loop robotic prototype.

Ethical Approval:

This study is based on a MATLAB engineering simulation using a computer-generated 3D heart mesh and synthetic sensor data, and does not involve human participants, animal subjects, patient data, or clinical intervention; therefore, ethical approval was not required.

Conflict of Interest

The authors declare that there are no conflicts of interest related to this study.

References

1. Bahlke, F. et al., 2024. First clinical data on artificial intelligence-guided catheter ablation in long-standing persistent atrial fibrillation. Journal of Cardiovascular Electrophysiology.
2. Aryana, A. and D'Avila, A., 2024. Emerging tools and techniques for catheter ablation of cardiac arrhythmias: A 2024 update. Journal of Innovations in Cardiac Rhythm Management.
3. Heart Rhythm Society, 2024. Clinical trial finds artificial intelligence-guided procedure for persistent atrial fibrillation superior to current standard of care: The TAILORED-AF randomized clinical trial. Presented at Heart Rhythm 2024, Boston, MA, USA.
4. Fox, D.J. et al., 2024. Impact of artificial intelligence arrhythmia mapping on time to first ablation, procedure duration, and fluoroscopy use. Journal of Cardiovascular Electrophysiology.
5. Ansari, Y., Mourad, O., Qaraqe, K. and Serpedin, E., 2023. Deep learning for ECG arrhythmia detection and classification: An overview of progress for period 2017–2023. Frontiers in Physiology, 14, art. 1246746.
6. Chauhan, V.S., Dubois, R., Gatti, D.L. and Zhao, J., 2025. Editorial: Advances in artificial intelligence-enhanced electrocardiography: A pathway towards improved diagnosis and patient care. Frontiers in Physiology.
7. European Heart Rhythm Association (EHRA), Heart Rhythm Society (HRS) and ESC Working Group on

E-Cardiology, 2025. State of the art of artificial intelligence in clinical electrophysiology in 2025: A scientific statement. EP Europace, 27(5), art. euaf071.
8. Lyu, H. et al., 2025. Lightweight deep learning architecture for multi-lead ECG arrhythmia detection. Sensors, 25(17), art. 5542.
9. An, X., Shi, S., Wang, Q., Yu, Y. and Liu, Q., 2024. Research on a lightweight arrhythmia classification model based on knowledge distillation for wearable single-lead ECG monitoring systems. Sensors, 24, art. 7896.
10. Mavaddati, S., 2025. ECG arrhythmias classification based on deep learning methods and transfer learning technique. Biomedical Signal Processing and Control, 101, art. 107236.
11. Li, Z., Lambranzi, C., Wu, D., Segato, A., De Marco, F., Vander Poorten, E., Dankelman, J. and De Momi, E., 2025. Robust path planning via learning from demonstrations for robotic catheters in deformable environments. IEEE Transactions on Biomedical Engineering, 72(1), pp.324–336.
12. Karstensen, L. et al., 2023. Recurrent neural networks for generalization towards the vessel geometry in autonomous endovascular guidewire navigation in the aortic arch. International Journal of Computer Assisted Radiology and Surgery, 18(9), pp.1735–1744.
13. Scarponi, V., Lecomte, F., Duprez, M., Nageotte, F. and Cotin, S., 2024. Autonomous guidewire navigation in dynamic environments. In Proceedings of the IEEE/RSJ International Conference on Intelligent Robots and Systems (IROS), pp.6931–6938.
14. Li, N., Wang, Y., Cheng, H., Zhao, H. and Ding, H., 2024. Vascular centerline-guided autonomous navigation methods for robot-led endovascular interventions. In Proceedings of the IEEE International Conference on Robotics and Automation (ICRA), pp.11578–11584.
15. Camps, J. et al., 2024. Digital twinning of the human ventricular activation sequence to clinical 12-lead ECGs and magnetic resonance imaging using realistic Purkinje networks for in silico clinical trials. Medical Image Analysis, 94, art. 103108.
16. Berg, L.A. et al., 2026. Toward cardiac electrophysiology digital twins with an efficient open source scalable solver on GPU clusters. Scientific Reports.
17. Grandits, T., Gillette, K., Plank, G. and Pezzuto, S., 2025. Accurate and efficient cardiac digital twin from surface ECGs: Insights into identifiability of ventricular conduction system. Medical Image Analysis, art. 103641.